International Journal of Innovative
Computing, Information and Control
Volume **14**, Number **1**, February **2018**

ICIC International ©2018 ISSN 1349-4198
pp. 33–52

ANTI-SATURATION DYNAMIC SURFACE CONTROL FOR SPACECRAFT TERMINAL SAFE APPROACH BASED ON COMMAND FILTER

Guanqun Wu, Shenmin Song* and Jingguang Sun

Center for Control Theory and Guidance Technology
Harbin Institute of Technology
No. 92, West Dazhi Street, Harbin 150001, P. R. China
{ wgqwuguanqun; sunjingguanghit }@163.com; *Corresponding author: songshenmin@hit.edu.cn

Received June 2017; revised October 2017

Abstract. *This paper studies anti-saturation control schemes of the spacecraft terminal safe approach. Based on the spacecraft relative motion model of terminal approach and spherical collision avoidance potential function, anti-saturation controller and adaptive anti-saturation controller are designed for the situations of known and unknown upper bound of external disturbances respectively using dynamic surface control (DSC) and auxiliary system. The designed controllers not only take advantage of the first-order command filter to avoid the differential of the virtual control signals, but also introduce the compensating signals to remove the effect of the error caused by the command filter. Under the proposed control strategies, the bounded and uniformly ultimate bounded of the system states are proved via Lyapunov stability theory, and the chaser can approach the desired position without collision with the target. The numerical simulations are conducted to demonstrate that the chaser spacecraft using the designed controllers can realize the terminal approach to the target safely, which further illustrate the effectiveness of the proposed controllers.*

Keywords: Terminal safe approach, Collision avoidance, Dynamic surface control, Command filter, Input saturation

1. **Introduction.** With the increasing of space strategy position, the spacecraft proximity relative motion control has become a research hotspot in space technology, which is being widely applied in many space missions, such as rendezvous and docking, on-orbit services and space attack-defense [1,2]. Considering the actual requirements as the external disturbances, input constraint and collision area, controlling the chaser to approach the target safely and accurately becomes the key to complete space missions. Consequently, the robust control of spacecraft proximity relative motion considering safety constraints has become an essential technology in aerospace [3].

Recently, experts and scholars at home and abroad have conducted a lot of research with respect to spacecraft relative motion control and obtained many important achievements [4-8]. On the basis of Tschauner-Hempel equations, a parametric Lyapunov differential equation method was proposed in [4] to solve the spacecraft rendezvous problem. In order to drive the chaser to approach the target, a modified adaptive controller with uncertain parameters was presented in [5], and the system states were proved asymptotic convergent with the controller. In [6], an integral sliding mode controller was proposed using linear quadratic optimal control theory to realize spacecraft hovering around elliptic orbits by tracking fuel-optimal trajectories. Contraposing spacecraft formation with uncertainties and disturbances, to improve the control precision of the system, an input-output linearization minimum sliding mode error feedback controller was designed in [7]. Using

back-stepping method, a robust adaptive controller was designed in [8] for spacecraft rendezvous and docking, with which the system states were globally uniformly ultimately bounded, and the uncertainties of the relative dynamics were compensated by using radial basis function neural networks.

Collision may happen in the process of the spacecraft relative motion. Thus, to ensure the safety of the chaser spacecraft, much literature considers collision avoidance in the design of relative motion control scheme [9-16]. For autonomous rendezvous and docking with a non-cooperative target, a new guidance control method using fuzzy logic combined with potential function was presented in [9] to ensure safe approaching. Aiming at spacecraft formation maintaining, new sliding mode controllers that used the special potential functions to realize avoiding obstacles were presented in [10]. For proximity operations of spacecraft formation flying near elliptic reference orbits, a tracking controller using Riccati procedure was provided in [11], also collision avoidance problem was settled via using Gaussian-like function. In [12], a nonlinear optimal control scheme was put forward using the optimal sliding mode control, which was combined with a quadratic function to keep away from moving obstacle. To realize accurate formation, finite-time controllers are designed for multiple Euler-Lagrange systems with avoiding obstacles using null-space-based and fast terminal sliding mode in [13]. As the in-depth study on the model predictive control (MPC), many control strategies based on MPC were put forward for rendezvous and docking with obstacle avoidance [14-16]. Robust control schemes based on explicit MPC and the linear quadratic MPC with dynamically reconfigurable constraints were proposed in [14,15], under which spacecraft rendezvous considering obstacle avoidance and a line-of-sight cone constraint can accomplish successfully. In [16], linear quadratic MPC and nonlinear MPC were applied for spacecraft rendezvous and docking, and multiple obstacles were avoided by using the controllers.

In the actual control system, the control force provided by the actuators is limited. The actuator saturation can weaken system control performance, even may result in system instability if the input saturation is not taken into consideration in the controller design. Thus, the problem of input saturation should be solved in the process of controller design [17-22]. The auxiliary system was introduced in [17] to analyze the effect of input saturation, with which adaptive tracking controllers were designed for MIMO systems with input saturation. Using the mean-value theorem, an adaptive fuzzy tracking controller was constructed in [18], which introduced a piecewise smooth function to approximate the saturation function. In [19], focusing on uncertain nonstrict-feedback systems, an adaptive fuzzy control scheme was proposed, and the problem of input saturation was solved by adopting an auxiliary design system. In [20], an auxiliary system was employed to deal with the influence of input constraints, combining with which robust back-stepping controller was presented for uncertain nonlinear systems with input constraints. Concentrating on spacecraft circular orbit rendezvous system subject to input saturation, a new robust gain scheduling controller was provided in [21]. For spacecraft rendezvous and proximity operations, a saturated adaptive back-stepping controller was put forward in [22], which adopted auxiliary design system for input saturation. The control strategies above can settle the problem of input constraint effectively, but there are a smaller number of control schemes with safe constraint considering input saturation at the same time.

In order to further research the spacecraft terminal safe approach control scheme considering input saturation, and being inspired by above research, anti-saturation controllers are designed using DSC and auxiliary system for the situations of known and unknown upper bound of external disturbances respectively, which use spherical collision avoidance

potential function to deal with taboo area in the chaser spacecraft motion. Compared with the above mentioned literature, the main contributions of the paper are as follows.

(1) The collision avoidance constraint is considered in terminal approach control. And the spherical collision avoidance potential function is introduced to make collision avoidance problem in terminal approach control be simplified into boundedness problem of reciprocal of the potential function.

(2) The proposed dynamic surface controllers use command filter to avoid the computations of time derivatives of the virtual control signals, and the compensating signals are introduced to remove the effects of the error caused by the command filter, which can improve the performance of the controllers.

(3) By introducing the auxiliary system, input saturation is taken into consideration in controller design to cope with physical constraints of the actuators, which makes the designed controllers have more practical value in engineering.

The rest of the paper is structured in following manner. Section 2 states a brief description of the spacecraft terminal safe approach control problem, including the target orbit coordinate system, spacecraft relative motion model of terminal approach, collision avoidance potential function and related assumptions for controller design. In Section 3, for the situations of known and unknown upper bound of external disturbances, two anti-saturation dynamic surface controllers are proposed respectively, and the Lyapunov theory is used to prove and analyze the performances of the controllers. Section 4 gives numerical simulations to further verify the effectiveness of the proposed controllers. Finally, the conclusions of the paper are presented in Section 5.

2. **Problem Formulation.**

2.1. **Spacecraft relative motion model of terminal approach.** The target orbit coordinate frame $F_t(O_t x_t y_t z_t)$ is shown in Figure 1. The origin of coordinate is the center of target. The positive direction of x_t axis is the direction that is from the center point to the target position. The positive direction of y_t axis points to the target movement direction. The positive direction of z_t axis is perpendicular to target orbital plane.

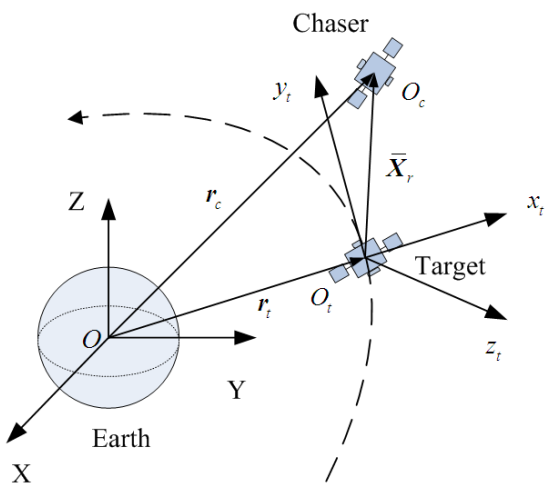

FIGURE 1. Target orbit coordinate frame

The dynamical equations of the chaser and the target in earth centered inertial (ECI) frame $F_o(OXYZ)$ are given as follows:

$$\ddot{\boldsymbol{r}}_c = -\frac{\mu \boldsymbol{r}_c}{r_c^3} + \frac{\boldsymbol{f}_{dc}}{m_c} + \frac{\overline{\boldsymbol{u}}}{m_c} \tag{1}$$

$$\ddot{\boldsymbol{r}}_t = -\frac{\mu \boldsymbol{r}_t}{r_t^3} + \frac{\boldsymbol{f}_{dt}}{m_t} \tag{2}$$

where $\boldsymbol{r}_c$ and $\boldsymbol{r}_t$ are defined as position vectors of the target and chaser in ECI frame $F_o(OXYZ)$ respectively, so the corresponding acceleration vectors are $\ddot{\boldsymbol{r}}_c$ and $\ddot{\boldsymbol{r}}_t$. $\overline{\boldsymbol{u}}$ is the control force of chaser. μ is the gravitational constant. $\boldsymbol{f}_{dc}$ and $\boldsymbol{f}_{dt}$ are all perturbation effects on the target and chaser. m_c and m_t are the mass of chaser and target.

Relative position vector in ECI frame can be defined as $\overline{\boldsymbol{X}}_r = \boldsymbol{r}_c - \boldsymbol{r}_t$; thus the relative acceleration vector $\ddot{\overline{\boldsymbol{X}}}_r$ can be obtained:

$$\ddot{\overline{\boldsymbol{X}}}_r = \ddot{\boldsymbol{r}}_c - \ddot{\boldsymbol{r}}_t = -\frac{\mu \boldsymbol{r}_c}{r_c^3} + \frac{\mu \boldsymbol{r}_t}{r_t^3} + \frac{\overline{\boldsymbol{u}}}{m_c} + \frac{\boldsymbol{f}_{dc}}{m_c} - \frac{\boldsymbol{f}_{dt}}{m_t} \tag{3}$$

Converting the $\ddot{\overline{\boldsymbol{X}}}_r$ into $F_t(O_t x_t y_t z_t)$ yields:

$$-\frac{\mu \boldsymbol{r}_c}{r_c^3} + \frac{\mu \boldsymbol{r}_t}{r_t^3} + \frac{\boldsymbol{u}}{m_c} + \frac{\boldsymbol{d}}{m_c} = \ddot{\boldsymbol{X}}_r + \boldsymbol{\omega}_t \times (\boldsymbol{\omega}_t \times \boldsymbol{X}_r) + \dot{\boldsymbol{\omega}}_t \times \boldsymbol{X}_r + 2\boldsymbol{\omega}_t \times \boldsymbol{X}_v \tag{4}$$

In Equation (4), $\boldsymbol{X}_r$ and $\ddot{\boldsymbol{X}}_r$ represent relative position vector and the relative acceleration vector in F_t, and $\boldsymbol{u}$ and disturbance $\boldsymbol{d}$ are denoted as $\overline{\boldsymbol{u}}$ and $\boldsymbol{f}_{dc} - \frac{m_c}{m_t}\boldsymbol{f}_{dt}$ in F_t.

In target orbit coordinate frame, define $\boldsymbol{X}_r = [x \;\; y \;\; z]^{\mathrm{T}}$ and $\boldsymbol{X}_v = \dot{\boldsymbol{X}}_r = [\dot{x} \;\; \dot{y} \;\; \dot{z}]^{\mathrm{T}}$. The angular velocity of the target is defined as $\boldsymbol{\omega}_t = [0 \;\; 0 \;\; \dot{\theta}_t]^{\mathrm{T}}$. The position vector from earth's core to the target and the chaser can be defined as $\boldsymbol{r}_t = [r_t \;\; 0 \;\; 0]^{\mathrm{T}}$ and $\boldsymbol{r}_c = [x + r_t \;\; y \;\; z]^{\mathrm{T}}$. Substituting the definition of the variables above into Equation (4), after simplification, spacecraft terminal approach relative motion model can be obtained as follows:

$$\begin{cases} \dot{\boldsymbol{X}}_r = \boldsymbol{X}_v \\ \dot{\boldsymbol{X}}_v = \boldsymbol{A}\boldsymbol{X}_v + \boldsymbol{B}\boldsymbol{X}_r + \boldsymbol{C} + \dfrac{\boldsymbol{d}}{m_c} + \dfrac{\boldsymbol{u}}{m_c} \end{cases} \tag{5}$$

where $\dot{\boldsymbol{X}}_v = [\ddot{x} \;\; \ddot{y} \;\; \ddot{z}]^{\mathrm{T}}$. $\boldsymbol{A}$, $\boldsymbol{B}$ and $\boldsymbol{C}$ are defined as follows:

$$\boldsymbol{A} = 2\dot{\theta}_t \begin{bmatrix} 0 & 1 & 0 \\ -1 & 0 & 0 \\ 0 & 0 & 0 \end{bmatrix} \tag{6}$$

$$\boldsymbol{B} = -\frac{\mu}{r_c^3}\boldsymbol{I}_{3\times 3} + \begin{bmatrix} \dot{\theta}_t^2 & \ddot{\theta}_t & 0 \\ -\ddot{\theta}_t & \dot{\theta}_t^2 & 0 \\ 0 & 0 & 0 \end{bmatrix} \tag{7}$$

$$\boldsymbol{C} = \mu \begin{bmatrix} \dfrac{1}{r_t^2} - \dfrac{r_t}{r_c^3} & 0 & 0 \end{bmatrix}^{\mathrm{T}} \tag{8}$$

where $\dot{\theta}_t = \frac{n_t(1+e_t\cos\theta_t)^2}{\left(1-e_t^2\right)^{3/2}}$, $\ddot{\theta}_t = \frac{-2n_t^2 e_t(1+e_t\cos\theta_t)^3\sin\theta_t}{\left(1-e_t^2\right)^3}$, and $n_t = \sqrt{\frac{\mu}{a_t^3}}$.

2.2. **Description of potential function and control objective.** In the process of accessing to the desired position, the chaser will be close to the target spacecraft within short distance, because collision may happen between the chaser and the target. To control the chaser to access to the desired position without collision, taboo area where collision can happen must be considered in the process. Taboo area in the paper is set

as sphere interior whose centre is the center of target and the radius is R. The collision avoidance potential function is presented as follows:

$$h(\boldsymbol{X}_r) = \frac{1}{R^2}\left(x^2 + y^2 + z^2 - R^2\right) \tag{9}$$

Assume $h(\boldsymbol{X}_{r0}) > 0$, that is, the initial position of the chaser is in safe area. In the process of approaching to the desired position, if the inequality $h(\boldsymbol{X}_r) > 0$ holds all the time, the chaser can realize terminal safe approach. On the contrary, if $h(\boldsymbol{X}_r) \leq 0$, the chaser may have collision with the target in the taboo area. Thus, if $h(\boldsymbol{X}_r) > 0$ holds from beginning to end, that is to say, the $1/h(\boldsymbol{X}_r)$ is bounded all the time, the chaser can approach desired position around the target safely.

Control objective: Aiming at the situation of known and unknown upper bound of external disturbances, two anti-saturation controllers should be designed respectively, under which the chaser can approach the expected position safely subject to input saturation constraint, that is, the relative position of the chaser $\boldsymbol{X}_r$ can convergence to the neighborhood of the desired location $\boldsymbol{X}_{rd}$, also $1/h(\boldsymbol{X}_r)$ is bounded all the time.

Remark 2.1. *The motivation of employing the potential function is to convert collision avoidance problem into boundedness problem of reciprocal of the potential function, and the designed controller combined with the potential function can guarantee the chaser complete the spacecraft terminal approach without collision happening.*

2.3. **Related lemmas and assumptions.** To facilitate the design and analysis of controller, related lemmas and assumptions are introduced as follows.

Lemma 2.1. [23]. *The compensating signals ξ_i $(i = 2, \ldots, n)$ are defined as follows*

$$\begin{aligned} \dot{\xi}_1 &= -c_1\xi_1 - \xi_1 + \xi_2 + (x_{2,c} - a_1) \\ \dot{\xi}_i &= -c_i\xi_i - \xi_{i-1} + \xi_{i+1} + (x_{i+1,c} - a_i) \\ \dot{\xi}_n &= -c_n\xi_n - \xi_{n-1} \end{aligned} \tag{10}$$

where $x_{i+1,c}$ and a_i are output and input of first-order command filter respectively. When $t \to \infty$ $\|\xi_i\|$ is bounded, satisfying $\lim\limits_{t\to\infty} \|\xi_i\| \leq \frac{\mu}{2k_0}$ where $k_0 = (1/2)\min(c_i)$.

Lemma 2.2. [17]. *For any arbitrary number x and non-zero real number y, then the following inequality holds*

$$0 \leq |x|\left(1 - \tanh(|x/y|)\right) \leq \alpha^* |y| \tag{11}$$

where $\alpha^* = 0.2785$.

Assumption 2.1. *The initial position and the desired position of the chaser $\boldsymbol{X}_{r0}$, $\boldsymbol{X}_{rd}$ are assumed to be set in safe area.*

Assumption 2.2. *The external disturbance $\boldsymbol{d}$ in Equation (5) is assumed to be bounded, and satisfies the inequality $\|\boldsymbol{d}\| \leq d_m$, where d_m is a positive constant.*

Remark 2.2. *For further on-orbit operation, the desired position $\boldsymbol{X}_{rd}$ should be in the safe area. Also, if the initial position $\boldsymbol{X}_{r0}$ is set in the taboo area, the chaser may have collided with the target. Thus, in order to design the controllers for the spacecraft terminal approach with collision avoidance, Assumption 2.1 is reasonable. In practice, the external disturbances are unknown but bounded which contain atmospheric drag, radiation pressure, etc. And [8,10,22] have presented assumptions similar to Assumption 2.2. Thus, Assumption 2.2 is reasonable.*

3. **Main Results.** For the spacecraft terminal approach relative motion model Equations (5)-(8), for the situations of known and unknown upper bound of external disturbances, two anti-saturation controllers are designed based on dynamic surface control with signal compensation and auxiliary system, by which the chaser can approach the desired position safely with input constraint.

3.1. **Anti-saturation controller design for the situation of known upper bound of external disturbances.** For the spacecraft terminal approach relative motion model Equations (5)-(8) with the known upper bound of external disturbances, the detailed processes of designing an anti-saturation controller are shown as follows.

Step 1: Define the tracking error variable $\boldsymbol{z}_1$ as follows:

$$\boldsymbol{z}_1 = \boldsymbol{X}_r - \boldsymbol{X}_{rd} \tag{12}$$

where $\boldsymbol{X}_{rd}$ is reference signal.

Computing the first order derivative of Equation (12):

$$\dot{\boldsymbol{z}}_1 = \dot{\boldsymbol{X}}_r - \dot{\boldsymbol{X}}_{rd} = \boldsymbol{X}_v - \dot{\boldsymbol{X}}_{rd} \tag{13}$$

Define the virtual control $\boldsymbol{\alpha}_{vc1}$ as follows:

$$\boldsymbol{\alpha}_{vc1} = -k_1 \boldsymbol{z}_1 \tag{14}$$

where k_1 is a positive constant.

To avoid the differential of the virtual control signal, the first order command filter is introduced as follows:

$$\tau_1 \dot{\boldsymbol{\alpha}}_{vd1} + \boldsymbol{\alpha}_{vd1} = \boldsymbol{\alpha}_{vc1}, \quad \boldsymbol{\alpha}_{vd1}(0) = \boldsymbol{\alpha}_{vc1}(0) \tag{15}$$

where $\boldsymbol{\alpha}_{vc1}$, $\boldsymbol{\alpha}_{vd1}$ are the input and output of the command filter respectively, and τ_1 is a positive constant.

To eliminate the effect of the error caused by the $\boldsymbol{\alpha}_{vd1} - \boldsymbol{\alpha}_{vc1}$, the compensating signal is introduced referring to Lemma 2.1. $\boldsymbol{\xi}_1$ is defined as follows:

$$\dot{\boldsymbol{\xi}}_1 = -k_1 \boldsymbol{\xi}_1 + \boldsymbol{\xi}_2 + (\boldsymbol{\alpha}_{vd1} - \boldsymbol{\alpha}_{vc1}) \tag{16}$$

Define the compensated tracking error signal $\boldsymbol{z}_{v1}$ as:

$$\boldsymbol{z}_{v1} = \boldsymbol{z}_1 - \boldsymbol{\xi}_1 \tag{17}$$

Choose Lyapunov function v_1 as:

$$v_1 = \frac{1}{2} \boldsymbol{z}_{v1}^T \boldsymbol{z}_{v1} \tag{18}$$

Compute the first order derivative of v_1:

$$\begin{aligned}
\dot{v}_1 &= \boldsymbol{z}_{v1}^T \dot{\boldsymbol{z}}_{v1} \\
&= \boldsymbol{z}_{v1}^T \left(\boldsymbol{X}_v - \dot{\boldsymbol{X}}_{rd} \right) + \boldsymbol{z}_{v1}^T \left(k_1 \boldsymbol{\xi}_1 - \boldsymbol{\xi}_2 - (\boldsymbol{\alpha}_{vd1} - \boldsymbol{\alpha}_{vc1}) \right) \\
&= \boldsymbol{z}_{v1}^T \left(\boldsymbol{z}_2 + \dot{\boldsymbol{X}}_{rd} + \boldsymbol{\alpha}_{vd1} - \dot{\boldsymbol{X}}_{rd} \right) + \boldsymbol{z}_{v1}^T \left(k_1 \boldsymbol{\xi}_1 - \boldsymbol{\xi}_2 - (\boldsymbol{\alpha}_{vd1} - \boldsymbol{\alpha}_{vc1}) \right) \\
&= \boldsymbol{z}_{v1}^T \left(\boldsymbol{z}_2 + \boldsymbol{\alpha}_{vc1} + \boldsymbol{\alpha}_{vd1} - \boldsymbol{\alpha}_{vc1} \right) + \boldsymbol{z}_{v1}^T \left(k_1 \boldsymbol{\xi}_1 - \boldsymbol{\xi}_2 - (\boldsymbol{\alpha}_{vd1} - \boldsymbol{\alpha}_{vc1}) \right) \\
&= \boldsymbol{z}_{v1}^T \left(\boldsymbol{z}_2 - k_1 \boldsymbol{z}_1 + k_1 \boldsymbol{\xi}_1 - \boldsymbol{\xi}_2 \right) \\
&= \boldsymbol{z}_{v1}^T \left(\boldsymbol{z}_2 - k_1 \boldsymbol{z}_{v1} - k_1 \boldsymbol{\xi}_1 + k_1 \boldsymbol{\xi}_1 - \boldsymbol{\xi}_2 \right) \\
&= -k_1 \boldsymbol{z}_{v1}^T \boldsymbol{z}_{v1} + \boldsymbol{z}_{v1}^T \left(\boldsymbol{z}_2 - \boldsymbol{\xi}_2 \right)
\end{aligned} \tag{19}$$

Step 2: Define the tracking error variable $\boldsymbol{z}_2$ as follows:

$$\boldsymbol{z}_2 = \boldsymbol{X}_v - \dot{\boldsymbol{X}}_{rd} - \boldsymbol{\alpha}_{vd1} \tag{20}$$

Computing the first order derivative of Equation (20) yields:

$$\dot{\boldsymbol{z}}_2 = \dot{\boldsymbol{X}}_v - \ddot{\boldsymbol{X}}_{rd} - \dot{\boldsymbol{\alpha}}_{vd1} = \boldsymbol{A}\boldsymbol{X}_v + \boldsymbol{B}\boldsymbol{X}_r + \boldsymbol{C} + \frac{\boldsymbol{d}}{m_c} + \frac{\boldsymbol{u}}{m_c} - \ddot{\boldsymbol{X}}_{rd} - \frac{1}{\tau_1}\left(\boldsymbol{\alpha}_{vc1} - \boldsymbol{\alpha}_{vd1}\right) \quad (21)$$

The compensating signal $\boldsymbol{\xi}_2$ is introduced as follows:

$$\dot{\boldsymbol{\xi}}_2 = -k_2\boldsymbol{\xi}_2 - \boldsymbol{\xi}_1 \quad (22)$$

where k_2 is a positive constant.

Define the compensated tracking error signal $\boldsymbol{z}_{v2}$ as:

$$\boldsymbol{z}_{v2} = \boldsymbol{z}_2 - \boldsymbol{\xi}_2 \quad (23)$$

Choose Lyapunov function v_2 as:

$$v_2 = \frac{1}{2}\boldsymbol{z}_{v2}^T\boldsymbol{z}_{v2} \quad (24)$$

Compute the first order derivative of v_2:

$$\dot{v}_2 = \boldsymbol{z}_{v2}^T\dot{\boldsymbol{z}}_{v2} = \boldsymbol{z}_{v2}^T\left(\boldsymbol{A}\boldsymbol{X}_v + \boldsymbol{B}\boldsymbol{X}_r + \boldsymbol{C} + \frac{\boldsymbol{d}}{m_c} + \frac{\boldsymbol{u}}{m_c} - \ddot{\boldsymbol{X}}_{rd} - \dot{\boldsymbol{\alpha}}_{vd1}\right) + \boldsymbol{z}_{v2}^T\left(k_2\boldsymbol{\xi}_2 + \boldsymbol{\xi}_1\right) \quad (25)$$

To handle input saturation, the auxiliary system Equation (26) is introduced:

$$\dot{\boldsymbol{\eta}} = \begin{cases} -k_\eta\boldsymbol{\eta} - \dfrac{1}{\|\boldsymbol{\eta}\|^2}\left(\dfrac{\left|\boldsymbol{z}_{v2}^T\cdot\Delta\boldsymbol{u}\right|}{m_c} + \dfrac{1}{2}\Delta\boldsymbol{u}^T\Delta\boldsymbol{u}\right)\boldsymbol{\eta} + \Delta\boldsymbol{u}, & \|\boldsymbol{\eta}\| \geq \sigma_V \\ 0, & \|\boldsymbol{\eta}\| < \sigma_V \end{cases} \quad (26)$$

where $\Delta\boldsymbol{u} = \boldsymbol{u} - \boldsymbol{u}_c$, $\boldsymbol{u}$ is the ideal control input, $\boldsymbol{u}_c$ is the actual control input, and σ_V is a positive constant.

For the situations that the upper bound of external disturbances is known, based on Equations (12)-(26), the controller is designed as Equation (27), where k_2, k_h, k_η, k_{h1} are positive constants, and inequalities $k_2 > \frac{1}{2}k_\eta$, $k_\eta > 1$ hold.

$$\boldsymbol{u}_c = m_c\begin{pmatrix} -k_2\boldsymbol{z}_2 - \boldsymbol{z}_1 - \boldsymbol{A}\boldsymbol{X}_v - \boldsymbol{B}\boldsymbol{X}_r - \boldsymbol{C} + \ddot{\boldsymbol{X}}_{rd} + \dot{\boldsymbol{\alpha}}_{vd1} - \dfrac{d_m}{m_c}\mathrm{sign}\left(\boldsymbol{z}_{v2}\right) \\ +k_\eta\boldsymbol{\eta} - k_h\dfrac{\boldsymbol{z}_{v2}}{\|\boldsymbol{z}_{v2}\|^2}\left(\dot{h}(\boldsymbol{X}_r)h^{-2}(\boldsymbol{X}_r) + k_{h1}h^{-1}(\boldsymbol{X}_r)\right) \end{pmatrix} \quad (27)$$

Theorem 3.1. *Consider the spacecraft terminal approach relative motion model Equations (5)-(8) with Assumption 2.1 and Assumption 2.2, for the situations of known upper bound of external disturbances, the state of the system is regulated under the designed controller Equation (27) and auxiliary system Equation (26), and the following conclusion can be drawn.*

(I) The variables v_1, v_2, $\boldsymbol{\eta}$, $1/h(\boldsymbol{X}_r)$ are bounded.

(II) The collision avoidance potential function $h(\boldsymbol{X}_r)$ is positive, that is, the chaser can avoid collision with the target in the process of motion.

(III) The tracking error variables $\boldsymbol{z}_1$, $\boldsymbol{z}_2$ can converge to any small neighborhood, that is, the relative position of the chaser $\boldsymbol{X}_r$ can converge to any small range of the desired position $\boldsymbol{X}_{rd}$.

Proof: Choose the Lyapunov function V_1 as:

$$V_1 = v_1 + v_2 + \frac{1}{2}\boldsymbol{\eta}^T\boldsymbol{\eta} + k_h\frac{1}{h(\boldsymbol{X}_r)} \quad (28)$$

Computing the derivative of V_1 yields:

$$\begin{aligned}
\dot{V}_1 &= \dot{v}_1 + \dot{v}_2 + \boldsymbol{\eta}^T\dot{\boldsymbol{\eta}} + k_h\frac{\dot{h}(\boldsymbol{X}_r)}{h^2(\boldsymbol{X}_r)} \\
&= -k_1\boldsymbol{z}_{v1}^T\boldsymbol{z}_{v1} + \boldsymbol{z}_{v1}^T(\boldsymbol{z}_2 - \boldsymbol{\xi}_2) + \boldsymbol{z}_{v2}^T\Bigg(\boldsymbol{A}\boldsymbol{X}_v + \boldsymbol{B}\boldsymbol{X}_r + \boldsymbol{C} + \frac{\boldsymbol{d}}{m_c} + \frac{\boldsymbol{u}_c}{m_c} \\
&\quad + \frac{\Delta\boldsymbol{u}}{m_c} - \ddot{\boldsymbol{X}}_{rd} - \dot{\boldsymbol{\alpha}}_{vd1}\Bigg) + \boldsymbol{z}_{v2}^T(k_2\boldsymbol{\xi}_2 + \boldsymbol{\xi}_1) + \boldsymbol{\eta}^T\dot{\boldsymbol{\eta}} + k_h\frac{\dot{h}(\boldsymbol{X}_r)}{h^2(\boldsymbol{X}_r)} \\
&= -k_1\boldsymbol{z}_{v1}^T\boldsymbol{z}_{v1} + \boldsymbol{z}_{v1}^T\boldsymbol{z}_{v2} + \boldsymbol{z}_{v2}^T(-k_2\boldsymbol{z}_2 - \boldsymbol{z}_1) + \boldsymbol{z}_{v2}^T(k_2\boldsymbol{\xi}_2 + \boldsymbol{\xi}_1) \\
&\quad + \boldsymbol{\eta}^T\dot{\boldsymbol{\eta}} + k_h\frac{\dot{h}(\boldsymbol{X}_r)}{h^2(\boldsymbol{X}_r)} + \boldsymbol{z}_{v2}^T\Bigg(\frac{\boldsymbol{d}}{m_c} + \frac{\Delta\boldsymbol{u}}{m_c} - \frac{d_m}{m_c}\mathrm{sign}(\boldsymbol{z}_{v2}) + k_\eta\boldsymbol{\eta} \\
&\quad - k_h\frac{\boldsymbol{z}_{v2}}{\|\boldsymbol{z}_{v2}\|^2}\left(\dot{h}(\boldsymbol{X}_r)h^{-2}(\boldsymbol{X}_r) + k_{h1}h^{-1}(\boldsymbol{X}_r)\right)\Bigg) \\
&= -k_1\boldsymbol{z}_{v1}^T\boldsymbol{z}_{v1} + \boldsymbol{z}_{v2}^T(\boldsymbol{z}_{v1} - k_2\boldsymbol{z}_2 - \boldsymbol{z}_1 + k_2\boldsymbol{\xi}_2 + \boldsymbol{\xi}_1) + \boldsymbol{\eta}^T\dot{\boldsymbol{\eta}} + k_h\frac{\dot{h}(\boldsymbol{X}_r)}{h^2(\boldsymbol{X}_r)} + \boldsymbol{z}_{v2}^T\Bigg(\frac{\boldsymbol{d}}{m_c} \\
&\quad + \frac{\Delta\boldsymbol{u}}{m_c} - \frac{d_m}{m_c}\mathrm{sign}(\boldsymbol{z}_{v2}) + k_\eta\boldsymbol{\eta} - k_h\frac{\boldsymbol{z}_{v2}}{\|\boldsymbol{z}_{v2}\|^2}\left(\dot{h}(\boldsymbol{X}_r)h^{-2}(\boldsymbol{X}_r) + k_{h1}h^{-1}(\boldsymbol{X}_r)\right)\Bigg) \\
&= -k_1\boldsymbol{z}_{v1}^T\boldsymbol{z}_{v1} - k_2\boldsymbol{z}_{v2}^T\boldsymbol{z}_{v2} - k_\eta\boldsymbol{\eta}^T\boldsymbol{\eta} - k_hk_{h1}\frac{1}{h(\boldsymbol{X}_r)} + \frac{\boldsymbol{z}_{v2}^T}{m_c}(\boldsymbol{d} - d_m\mathrm{sign}(\boldsymbol{z}_{v2})) \\
&\quad + k_\eta\boldsymbol{z}_{v2}^T\boldsymbol{\eta} + \boldsymbol{z}_{v2}^T\frac{\Delta\boldsymbol{u}}{m_c} - \left(\frac{\left|\boldsymbol{z}_{v2}^T\Delta\boldsymbol{u}\right|}{m_c} + \frac{1}{2}\Delta\boldsymbol{u}^T\Delta\boldsymbol{u}\right) + \boldsymbol{\eta}^T\Delta\boldsymbol{u}
\end{aligned} \tag{29}$$

Two inequalities can be derived:

$$\boldsymbol{z}_{v2}^T\Delta\boldsymbol{u} - \left|\boldsymbol{z}_{v2}^T\Delta\boldsymbol{u}\right| \le 0 \tag{30}$$

$$\begin{aligned}
k_\eta\boldsymbol{z}_{v2}^T\boldsymbol{\eta} + \boldsymbol{\eta}^T\Delta\boldsymbol{u} &= k_\eta\sum_{i=1}^{3} z_{v2,i}\eta_i + \sum_{i=1}^{3}\Delta u_i\eta_i \\
&\le \frac{1}{2}k_\eta\boldsymbol{z}_{v2}^T\boldsymbol{z}_{v2} + \frac{1}{2}(k_\eta + 1)\boldsymbol{\eta}^T\boldsymbol{\eta} + \frac{1}{2}\Delta\boldsymbol{u}^T\Delta\boldsymbol{u}
\end{aligned} \tag{31}$$

Substituting Equations (30) and (31) into Equation (29), then Equation (29) can be rewritten as:

$$\begin{aligned}
\dot{V}_1 &\le -k_1\boldsymbol{z}_{v1}^T\boldsymbol{z}_{v1} - \left(k_2 - \frac{1}{2}k_\eta\right)\boldsymbol{z}_{v2}^T\boldsymbol{z}_{v2} - \left(\frac{1}{2}k_\eta - \frac{1}{2}\right)\boldsymbol{\eta}^T\boldsymbol{\eta} - k_hk_{h1}\frac{1}{h(\boldsymbol{X}_r)} \\
&\quad + \frac{\boldsymbol{z}_{v2}^T}{m_c}(\boldsymbol{d} - d_m\mathrm{sign}(\boldsymbol{z}_{v2})) \\
&\le -k_1\boldsymbol{z}_{v1}^T\boldsymbol{z}_{v1} - \left(k_2 - \frac{1}{2}k_\eta\right)\boldsymbol{z}_{v2}^T\boldsymbol{z}_{v2} - \left(\frac{1}{2}k_\eta - \frac{1}{2}\right)\boldsymbol{\eta}^T\boldsymbol{\eta} - k_hk_{h1}\frac{1}{h(\boldsymbol{X}_r)} \\
&\quad + \frac{\|\boldsymbol{z}_{v2}\|}{m_c}(\|\boldsymbol{d}\| - d_m) \\
&\le -k_1\boldsymbol{z}_{v1}^T\boldsymbol{z}_{v1} - \left(k_2 - \frac{1}{2}k_\eta\right)\boldsymbol{z}_{v2}^T\boldsymbol{z}_{v2} - \left(\frac{1}{2}k_\eta - \frac{1}{2}\right)\boldsymbol{\eta}^T\boldsymbol{\eta} - k_hk_{h1}\frac{1}{h(\boldsymbol{X}_r)} \\
&\le -\varepsilon_1 V_1
\end{aligned} \tag{32}$$

where $\varepsilon_1 = \min\left\{2k_1, 2\left(k_2 - \frac{1}{2}k_\eta\right), 2\left(\frac{1}{2}k_\eta - \frac{1}{2}\right), k_{h1}\right\}$, $k_2 > \frac{1}{2}k_\eta$, $k_\eta > 1$.

Equation (32) shows that $\dot{V}_1 \leq 0$, so V_1 is not increasing, which means that v_1, v_2, $\boldsymbol{\eta}$, $1/h(\boldsymbol{X}_r)$ are bounded.

Because initial value $h(\boldsymbol{X}_{r0})$ is positive and $1/h(\boldsymbol{X}_r)$ is bounded, it can be obtained that $h(\boldsymbol{X}_r) \neq 0$ holds during the change of the system states, which indicates that collision avoidance potential function $h(\boldsymbol{X}_r)$ is not equal to zero in the process of approaching the target, that is to say, the chaser moves in safe area all the time and can realize spacecraft terminal approach safely.

Therefore, conclusions (I) and (II) have been proved.

According to Equation (32), inequality can be obtained as:

$$V_1(t) \leq V_1(0)e^{-\varepsilon_1 t} \tag{33}$$

From Equation (33), it can be obtained that v_1, $v_2 \leq V_1(0)e^{-\varepsilon_1 t}$. When $t \to \infty$, $v_1, v_2 \to 0$, further $\boldsymbol{z}_{v1}$, $\boldsymbol{z}_{v2} \to 0$. From Lemma 2.1 it can be seen that $\boldsymbol{\xi}_1$ and $\boldsymbol{\xi}_2$ are bounded. So when ε_1 is selected large enough, the tracking error variables $\boldsymbol{z}_1$, $\boldsymbol{z}_2$ can converge to any small neighborhood.

Therefore, conclusion (III) has been proved.

The proof of Theorem 3.1 has been completed.

Remark 3.1. *The use of command filter may cause the filtering errors which can lead to great tracking error. Therefore, the thesis introduces the compensating signals Equation (16) and Equation (22) to remove the effect of the error caused by the command filter so that the tracking error can be diminished.*

Remark 3.2. *Generally, the upper bound of external disturbances of the system is unknown because of the complex external environment; thus the controller Equation (27) results in failure. To make the control scheme more valuable to practice, an adaptive controller is designed as the following.*

3.2. **Adaptive anti-saturation controller design for the situation of unknown upper bound of external disturbances.** To deal with the spacecraft terminal approach with unknown upper bound of external disturbances, the paper further designs an adaptive anti-saturation controller.

Based on Equations (12)-(26) derived using DSC, command filter and the compensating signal, a novel controller Equation (34) is designed which adopts adaptive law Equations (35) and (36) to estimate the upper bound of unknown external disturbances, where k_2, k_3, k_h, k_η, γ_d are positive constants, and inequalities $k_2 > \frac{1}{2}k_\eta$, $k_\eta > 1$ hold, $\hat{d}_m$ is the estimation value of upper bound of external disturbances d_m.

$$\boldsymbol{u}_c = m_c \begin{pmatrix} -k_2\boldsymbol{z}_2 - \boldsymbol{z}_1 - \boldsymbol{A}\boldsymbol{X}_v - \boldsymbol{B}\boldsymbol{X}_r - \boldsymbol{C} + \ddot{\boldsymbol{X}}_{rd} + \dot{\boldsymbol{\alpha}}_{vd1} \\ -\dfrac{\hat{d}_m}{m_c}\tanh\left(\boldsymbol{z}_{v2}/p_V^2\right) + k_\eta\boldsymbol{\eta} - k_h\dfrac{\boldsymbol{z}_{v2}}{\|\boldsymbol{z}_{v2}\|^2}\left(\dot{h}(\boldsymbol{X}_r)h^{-2}(\boldsymbol{X}_r) + h^{-1}(\boldsymbol{X}_r)\right) \end{pmatrix} \tag{34}$$

$$\dot{\hat{d}}_m = \gamma_d \|\boldsymbol{z}_{v2}\|_1 \tag{35}$$

$$\frac{\mathrm{d}}{\mathrm{dt}}p_V^2 = -3k_3\alpha^*\hat{d}_m p_V^2 \tag{36}$$

Theorem 3.2. *Consider the spacecraft terminal approach relative motion model Equations (5)-(8) with Assumption 2.1 and Assumption 2.2, for the situations of unknown upper bound of external disturbances, the state of the system is regulated under the designed adaptive controller Equation (34), adaptive law Equations (35) and (36) and auxiliary system Equation (26), the following conclusion can be drawn.*

(I) The collision avoidance potential function $h(\boldsymbol{X}_r)$ is positive, that is, the chaser can avoid collision with the target in the process of motion.

(II) The variables v_1, v_2, $\boldsymbol{\eta}$, $1/h(\boldsymbol{X}_r)$ are uniformly ultimately bounded.

(III) The tracking error variables $\boldsymbol{z}_1$, $\boldsymbol{z}_2$ can converge to any small neighborhood, that is, the relative position of the chaser $\boldsymbol{X}_r$ can converge to any small range of the desired position $\boldsymbol{X}_{rd}$.

Proof: Choose the Lyapunov function candidate as

$$V_2 = v_1 + v_2 + \frac{1}{2}\boldsymbol{\eta}^T\boldsymbol{\eta} + \frac{1}{2\gamma_d m_c}\tilde{d}_m^2 + \frac{1}{m_c k_3}p_V^2 + k_h\frac{1}{h(\boldsymbol{X}_r)} \tag{37}$$

where $\tilde{d}_m$ is the estimation error $\tilde{d}_m = d_m - \hat{d}_m$ of upper bound of external disturbances.

Computing the derivative of V_2 yields:

$$\begin{aligned}
\dot{V}_2 =& \dot{v}_1 + \dot{v}_2 + \boldsymbol{\eta}^T\dot{\boldsymbol{\eta}} + \frac{1}{\gamma_d m_c}\tilde{d}_m\dot{\tilde{d}}_m + \frac{1}{m_c k_3}\frac{\mathrm{d}}{\mathrm{dt}}p_V^2 + k_h\frac{\dot{h}(\boldsymbol{X}_r)}{h^2(\boldsymbol{X}_r)} \\
=& -k_1\boldsymbol{z}_{v1}^T\boldsymbol{z}_{v1} + \boldsymbol{z}_{v1}^T(\boldsymbol{z}_2 - \boldsymbol{\xi}_2) + \boldsymbol{z}_{v2}^T\Bigg(\boldsymbol{A}\boldsymbol{X}_v + \boldsymbol{B}\boldsymbol{X}_r + \boldsymbol{C} + \frac{\boldsymbol{d}}{m_c} + \frac{\boldsymbol{u}_c}{m_c} + \frac{\Delta\boldsymbol{u}}{m_c} \\
& - \ddot{\boldsymbol{X}}_{rd} - \dot{\boldsymbol{\alpha}}_{vd1}\Bigg) + \boldsymbol{z}_{v2}^T(k_2\boldsymbol{\xi}_2 + \boldsymbol{\xi}_1) + \boldsymbol{\eta}^T\dot{\boldsymbol{\eta}} + \frac{1}{\gamma_d m_c}\tilde{d}_m\dot{\tilde{d}}_m + \frac{1}{m_c}\frac{\mathrm{d}}{\mathrm{dt}}p_V^2 + k_h\frac{\dot{h}(\boldsymbol{X}_r)}{h^2(\boldsymbol{X}_r)} \\
=& -k_1\boldsymbol{z}_{v1}^T\boldsymbol{z}_{v1} + \boldsymbol{z}_{v1}^T\boldsymbol{z}_{v2} + \boldsymbol{z}_{v2}^T(-k_2\boldsymbol{z}_2 - \boldsymbol{z}_1) + \boldsymbol{z}_{v2}^T(k_2\boldsymbol{\xi}_2 + \boldsymbol{\xi}_1) \\
& + \boldsymbol{z}_{v2}^T\Bigg(\frac{\boldsymbol{d}}{m_c} + \frac{\Delta\boldsymbol{u}}{m_c} - \frac{\hat{d}_m}{m_c}\tanh\left(\boldsymbol{z}_{v2}/p_V^2\right) + k_\eta\boldsymbol{\eta} - k_h\frac{\boldsymbol{z}_{v2}}{\|\boldsymbol{z}_{v2}\|^2}\Big(\dot{h}(\boldsymbol{X}_r)h^{-2}(\boldsymbol{X}_r) \\
& + h^{-1}(\boldsymbol{X}_r)\Big)\Bigg) + \boldsymbol{\eta}^T\dot{\boldsymbol{\eta}} + \frac{1}{\gamma_d m_c}\tilde{d}_m\dot{\tilde{d}}_m + \frac{1}{m_c k_3}\frac{\mathrm{d}}{\mathrm{dt}}p_V^2 + k_h\frac{\dot{h}(\boldsymbol{X}_r)}{h^2(\boldsymbol{X}_r)} \\
=& -k_1\boldsymbol{z}_{v1}^T\boldsymbol{z}_{v1} - k_2\boldsymbol{z}_{v2}^T\boldsymbol{z}_{v2} - k_\eta\boldsymbol{\eta}^T\boldsymbol{\eta} - k_h\frac{1}{h(\boldsymbol{X}_r)} + \frac{\boldsymbol{z}_{v2}^T}{m_c}\left(\boldsymbol{d} - \hat{d}_m\tanh\left(\boldsymbol{z}_{v2}/p_V^2\right)\right) \\
& + k_h\boldsymbol{z}_{v2}^T + k_\eta\boldsymbol{z}_{v2}^T\boldsymbol{\eta} + \boldsymbol{z}_{v2}^T\frac{\Delta\boldsymbol{u}}{m_c} - \left(\frac{\left|\boldsymbol{z}_{v2}^T\Delta\boldsymbol{u}\right|}{m_c} + \frac{1}{2}\Delta\boldsymbol{u}^T\Delta\boldsymbol{u}\right) + \boldsymbol{\eta}^T\Delta\boldsymbol{u} \\
& + \frac{1}{\gamma_d m_c}\tilde{d}_m\dot{\tilde{d}}_m + \frac{1}{m_c k_3}\frac{\mathrm{d}}{\mathrm{dt}}p_V^2
\end{aligned} \tag{38}$$

Because Equations (30) and (31) hold, Equation (38) can be further rewritten as:

$$\begin{aligned}
\dot{V}_2 \le& -k_1\boldsymbol{z}_{v1}^T\boldsymbol{z}_{v1} - \left(k_2 - \frac{1}{2}k_\eta\right)\boldsymbol{z}_{v2}^T\boldsymbol{z}_{v2} - \left(\frac{1}{2}k_\eta - \frac{1}{2}\right)\boldsymbol{\eta}^T\boldsymbol{\eta} - k_h\frac{1}{h(\boldsymbol{X}_r)} \\
& + \frac{\boldsymbol{z}_{v2}^T}{m_c}\left(\boldsymbol{d} - \hat{d}_m\tanh\left(\boldsymbol{z}_{v2}/p_V^2\right)\right) + \frac{1}{\gamma_d m_c}\tilde{d}_m\dot{\tilde{d}}_m + \frac{1}{m_c k_3}\frac{\mathrm{d}}{\mathrm{dt}}p_V^2
\end{aligned} \tag{39}$$

According to Lemma 2.2 and Assumption 2.2, the following inequality can be derived:

$$\begin{aligned}
& \frac{1}{m_c}\left(\boldsymbol{z}_{v2}^T\boldsymbol{d} - \hat{d}_m\boldsymbol{z}_{v2}^T\tanh\left(\boldsymbol{z}_{v2}/p_V^2\right)\right) \\
\le& \frac{1}{m_c}\sum_{i=1}^{3}\left(z_{v2,i}d_i + \hat{d}_m p_V^2\left(\alpha^* - \left|z_{v2,i}\right|/p_V^2\right)\right) \\
\le& \frac{1}{m_c}\sum_{i=1}^{3}\left(\left|z_{v2,i}\right|d_m + \hat{d}_m p_V^2\left(\alpha^* - \left|z_{v2,i}\right|/p_V^2\right)\right) \\
\le& \frac{1}{m_c}\left(3\alpha^*\hat{d}_m p_V^2 + \tilde{d}_m\sum_{i=1}^{3}\left|z_{v2,i}\right|\right)
\end{aligned} \tag{40}$$

Substituting Equation (40) into Equation (39) yields

$$\begin{aligned}\dot{V}_2 \leq & -k_1\boldsymbol{z}_{v1}^T\boldsymbol{z}_{v1} - \left(k_2 - \frac{1}{2}k_\eta\right)\boldsymbol{z}_{v2}^T\boldsymbol{z}_{v2} - \left(\frac{1}{2}k_\eta - \frac{1}{2}\right)\boldsymbol{\eta}^T\boldsymbol{\eta} - k_h\frac{1}{h(\boldsymbol{X}_r)} \\ & + \frac{1}{m_c}\left(3\alpha^*\hat{d}_m p_V^2 + \tilde{d}_m\sum_{i=1}^{3}|z_{v2,i}|\right) - \frac{1}{\gamma_d m_c}\tilde{d}_m\dot{\hat{d}}_m - \frac{3\alpha^*\hat{d}_m p_V^2}{m_c} \\ = & -k_1\boldsymbol{z}_{v1}^T\boldsymbol{z}_{v1} - \left(k_2 - \frac{1}{2}k_\eta\right)\boldsymbol{z}_{v2}^T\boldsymbol{z}_{v2} - \left(\frac{1}{2}k_\eta - \frac{1}{2}\right)\boldsymbol{\eta}^T\boldsymbol{\eta} - k_h\frac{1}{h(\boldsymbol{X}_r)} \\ & + \frac{1}{m_c}\left(\tilde{d}_m\sum_{i=1}^{3}|z_{v2,i}| - \tilde{d}_m\|\boldsymbol{z}_{v2}\|_1\right) \\ = & -k_1\boldsymbol{z}_{v1}^T\boldsymbol{z}_{v1} - \left(k_2 - \frac{1}{2}k_\eta\right)\boldsymbol{z}_{v2}^T\boldsymbol{z}_{v2} - \left(\frac{1}{2}k_\eta - \frac{1}{2}\right)\boldsymbol{\eta}^T\boldsymbol{\eta} - k_h\frac{1}{h(\boldsymbol{X}_r)} \\ \leq & \ 0\end{aligned} \tag{41}$$

Equation (41) shows that $\dot{V}_2 \leq 0$, so V_2 is not increasing, which means that v_1, v_2, $\boldsymbol{\eta}$, $\tilde{d}_m$, $1/h(\boldsymbol{X}_r)$ are bounded. Therefore, the estimated value of the adaptive parameter $\hat{d}_m$ is bounded. That is to say, there exists a positive constant $\overline{d}_m > 0$ satisfying $\hat{d}_m \leq \overline{d}_m$.

Because initial value $h(\boldsymbol{X}_{r0})$ is positive and $1/h(\boldsymbol{X}_r)$ is bounded, it can be concluded that $h(\boldsymbol{X}_r) \neq 0$ holds during the change of the system states, which indicates that collision avoidance potential function $h(\boldsymbol{X}_r)$ is not equal to zero in the process of approaching the target, that is to say, the chaser moves in safe area all the time.

In order to further analyze the performance of the controller Equation (34), Lyapunov function V_3 is chosen as

$$V_3 = v_1 + v_2 + \frac{1}{2}\boldsymbol{\eta}^T\boldsymbol{\eta} + \frac{1}{2\gamma_d m_c}\left(\overline{d}_m - \hat{d}_m\right)^2 + \frac{2}{m_c k_3}p_V^2 + k_h\frac{1}{h(\boldsymbol{X}_r)} \tag{42}$$

Compute the derivative of Equation (42):

$$\begin{aligned}\dot{V}_3 = & -k_1\boldsymbol{z}_{v1}^T\boldsymbol{z}_{v1} + \boldsymbol{z}_{v1}^T\boldsymbol{z}_{v2} + \boldsymbol{z}_{v2}^T\left(-k_2\boldsymbol{z}_2 - \boldsymbol{z}_1\right) + \boldsymbol{z}_{v2}^T\left(k_2\boldsymbol{\xi}_2 + \boldsymbol{\xi}_1\right) + \boldsymbol{\eta}^T\dot{\boldsymbol{\eta}} \\ & + \frac{1}{\gamma_d m_c}\left(\overline{d}_m - \hat{d}_m\right)\dot{\hat{d}}_m + \boldsymbol{z}_{v2}^T\left(\frac{\boldsymbol{d}}{m_c} + \frac{\Delta\boldsymbol{u}}{m_c} - \frac{\hat{d}_m}{m_c}\tanh\left(\boldsymbol{z}_{v2}/p_V^2\right) + k_\eta\boldsymbol{\eta}\right. \\ & \left. - k_h\frac{\boldsymbol{z}_{v2}}{\boldsymbol{z}_{v2}^T\boldsymbol{z}_{v2}}h^{-1}(\boldsymbol{X}_r)\right) + \frac{2}{m_c k_3}\frac{\mathrm{d}}{\mathrm{d}t}p_V^2 \\ = & -k_1\boldsymbol{z}_{v1}^T\boldsymbol{z}_{v1} - k_2\boldsymbol{z}_{v2}^T\boldsymbol{z}_{v2} - k_\eta\boldsymbol{\eta}^T\boldsymbol{\eta} - k_h\frac{1}{h(\boldsymbol{X}_r)} + \frac{\boldsymbol{z}_{v2}^T}{m_c}\left(\boldsymbol{d} - \hat{d}_m\tanh\left(\boldsymbol{z}_{v2}/p_V^2\right)\right) \\ & + k_\eta\boldsymbol{z}_{v2}^T\boldsymbol{\eta} + \boldsymbol{z}_{v2}^T\frac{\Delta\boldsymbol{u}}{m_c} - \left(\frac{\left|\boldsymbol{z}_{v2}^T\Delta\boldsymbol{u}\right|}{m_c} + \frac{1}{2}\Delta\boldsymbol{u}^T\Delta\boldsymbol{u}\right) + \boldsymbol{\eta}^T\Delta\boldsymbol{u} \\ & + \frac{1}{\gamma_d m_c}\left(\overline{d}_m - \hat{d}_m\right)\dot{\hat{d}}_m + \frac{2}{m_c k_3}\frac{\mathrm{d}}{\mathrm{d}t}p_V^2 \\ \leq & -k_1\boldsymbol{z}_{v1}^T\boldsymbol{z}_{v1} - \left(k_2 - \frac{1}{2}k_\eta\right)\boldsymbol{z}_{v2}^T\boldsymbol{z}_{v2} - \left(\frac{1}{2}k_\eta - \frac{1}{2}\right)\boldsymbol{\eta}^T\boldsymbol{\eta} - k_h\frac{1}{h(\boldsymbol{X}_r)} \\ & + \frac{\boldsymbol{z}_{v2}^T}{m_c}\left(\boldsymbol{d} - \hat{d}_m\tanh\left(\boldsymbol{z}_{v2}/p_V^2\right)\right) + \frac{1}{\gamma_d m_c}\left(\overline{d}_m - \hat{d}_m\right)\dot{\hat{d}}_m + \frac{2}{m_c k_3}\frac{\mathrm{d}}{\mathrm{d}t}p_V^2\end{aligned} \tag{43}$$

According to Lemma 2.2, Assumption 2.2 and $\hat{d}_m \leq \overline{d}_m$, the inequality can be derived:

$$\begin{aligned}
&\frac{1}{m_c}\left(\boldsymbol{z}_{v2}^T\boldsymbol{d} - \hat{d}_m\boldsymbol{z}_{v2}^T\tanh\left(\boldsymbol{z}_{v2}/p_V^2\right)\right)\\
&= \frac{1}{m_c}\sum_{i=1}^{3} z_{v2,i}\left(d_i - \hat{d}_m\tanh\left(z_{v2,i}/p_V^2\right)\right)\\
&\leq \frac{1}{m_c}\sum_{i=1}^{3}\left(z_{v2,i}\overline{d}_m + \hat{d}_m p_V^2\left(\alpha^* - \left|z_{v2,i}\right|/p_V^2\right)\right)\\
&\leq \frac{1}{m_c}\left(3\alpha^*\hat{d}_m p_V^2 + \left(\overline{d}_m - \hat{d}_m\right)\sum_{i=1}^{3}\left|z_{v2,i}\right|\right)
\end{aligned} \tag{44}$$

Substituting Equation (44) into Equation (43) yields:

$$\begin{aligned}
\dot{V}_3 \leq & -k_1\boldsymbol{z}_{v1}^T\boldsymbol{z}_{v1} - \left(k_2 - \frac{1}{2}k_\eta\right)\boldsymbol{z}_{v2}^T\boldsymbol{z}_{v2} - \left(\frac{1}{2}k_\eta - \frac{1}{2}\right)\boldsymbol{\eta}^T\boldsymbol{\eta} - k_h\frac{1}{h(\boldsymbol{X}_r)}\\
& - \frac{1}{2\gamma_d m_c}\left(\overline{d}_m - \hat{d}_m\right)^2 - \frac{1}{m_c}p_V^2 + \frac{1}{2\gamma_d m_c}\left(\overline{d}_m - \hat{d}_m\right)^2\\
\leq & -\varepsilon_2 V_3 + C_1
\end{aligned} \tag{45}$$

where $\varepsilon_2 = \min\left\{2k_1, 2\left(k_2 - \frac{1}{2}k_\eta\right), 2\left(\frac{1}{2}k_\eta - \frac{1}{2}\right), \frac{k_3}{2}, 1\right\}$, $k_2 > \frac{1}{2}k_\eta$, $k_\eta > 1$, $C_1 = \frac{1}{2\gamma_d m_c}\left(\overline{d}_m - \hat{d}_m\right)^2$ is bounded. From Equation (45), it can be known that v_1, v_2, $\boldsymbol{\eta}$, $1/h(\boldsymbol{X}_r)$ are uniformly ultimately bounded.

Therefore, conclusion (II) has been proved.

According to Equation (45), inequality can be derived:

$$0 \leq V_3(t) \leq \left(V_3(0) - \frac{C_1}{\varepsilon_2}\right)e^{-\varepsilon_2 t} + \frac{C_1}{\varepsilon_2} \tag{46}$$

From Equation (46), it can be known v_1, $v_2 \leq \left(V_3(0) - \frac{C_1}{\varepsilon_2}\right)e^{-\varepsilon_2 t} + \frac{C_1}{\varepsilon_2}$. When $t \to \infty$, $v_1, v_2 \to \frac{C_1}{\varepsilon_2}$, further it can be got $\lim_{t\to\infty}\|\boldsymbol{z}_{v1}\| = \sqrt{\frac{2C_1}{\varepsilon_2}}$, $\lim_{t\to\infty}\|\boldsymbol{z}_{v2}\| = \sqrt{\frac{2C_1}{\varepsilon_2}}$. From Lemma 2.1, it can be seen that $\boldsymbol{\xi}_1$ and $\boldsymbol{\xi}_2$ are bounded, so when ε_2 is selected large enough, the tracking error variables $\boldsymbol{z}_1$, $\boldsymbol{z}_2$ can converge to any small neighborhood.

Therefore, conclusion (III) has been proved.

The proof of Theorem 3.2 has been completed.

Remark 3.3. *The auxiliary systems Equation (26) used in control schemes can handle input saturation problem for the cases that the input saturation is symmetrical and asymmetric.*

Remark 3.4. *Considering the anti-saturation controller Equation (27) and adaptive anti-saturation controller Equation (34), if error $\boldsymbol{z}_{v2}$ converges to zero infinitely, singularity problem may appear in the system. In the simulation analysis, the controller Equation (27) and the controller Equation (34) are modified to Equation (47) and Equation (48) respectively to avoid the phenomenon:*

$$\boldsymbol{u}_c = m_c\begin{pmatrix} -k_2\boldsymbol{z}_2 - \boldsymbol{z}_1 - \boldsymbol{A}\boldsymbol{X}_v - \boldsymbol{B}\boldsymbol{X}_r - \boldsymbol{C} + \ddot{\boldsymbol{X}}_{rd} + \dot{\boldsymbol{\alpha}}_{vd1} - \dfrac{d_m}{m_c}\operatorname{sign}\left(\boldsymbol{z}_{v2}\right)\\ +k_\eta\boldsymbol{\eta} - k_h\dfrac{\boldsymbol{z}_{v2}}{\left\|\boldsymbol{z}_{v2}\right\|^2 + \Delta}\left(\dot{h}(\boldsymbol{X}_r)h^{-2}(\boldsymbol{X}_r) + k_{h1}h^{-1}(\boldsymbol{X}_r)\right)\end{pmatrix} \tag{47}$$

$$\boldsymbol{u}_c = m_c \begin{pmatrix} -k_2\boldsymbol{z}_2 - \boldsymbol{z}_1 - \boldsymbol{A}\boldsymbol{X}_v - \boldsymbol{B}\boldsymbol{X}_r - \boldsymbol{C} + \ddot{\boldsymbol{X}}_{rd} + \dot{\boldsymbol{\alpha}}_{vd1} \\ -\dfrac{\hat{d}_m}{m_c}\tanh\left(\boldsymbol{z}_{v2}/p_V^2\right) + k_\eta\boldsymbol{\eta} - k_h\dfrac{\boldsymbol{z}_{v2}}{\|\boldsymbol{z}_{v2}\|^2 + \Delta}\left(\dot{h}(\boldsymbol{X}_r)h^{-2}(\boldsymbol{X}_r) + h^{-1}(\boldsymbol{X}_r)\right) \end{pmatrix} \tag{48}$$

where Δ is a very small positive constant.

4. **Simulation Analysis.** In order to validate the effectiveness of the designed controllers, simulations are conducted in this section for the situations that the upper bound of the external disturbances is known and unknown respectively.

In the process of simulations, to make these parameters more reasonable, the values of the basis parameters refer to the values of the corresponding parameters in [10]. The detailed names and values of parameters are shown in Table 1.

Table 1. Parts of parameters for simulation

Parameter	Value
The maximum input force	$5N$
The mass of the chaser	$m_c = 120$ kg
The orbital element of the target: Semi-major axis	$a = 7.0 \times 10^6$ km
The orbital element of the target: Eccentricity	$e = 0.02$
The orbital element of the target: Longitude ascending node	$\Omega = 50 \times \pi/180$ rad
The orbital element of the target: Inclination	$i = 40 \times \pi/180$ rad
The orbital element of the target: Argument of perigee	$\omega = 45 \times \pi/180$ rad
The orbital element of the target: Initial true anomaly	$f = 10$ rad

The initial relative speed vector and the desired relative speed vector are assumed as $\boldsymbol{X}_{v0} = [0\ \ 0\ \ 0]^{\mathrm{T}}$ m/s and $\boldsymbol{X}_{vd} = [0\ \ 0\ \ 0]^{\mathrm{T}}$ m/s. To verify the effectiveness and robustness of the controller, simulations for two cases are conducted.

Case1: The radius of the sphere in collision avoidance potential and the external disturbances are set as $R = 10$ m and $\boldsymbol{d} = 10^{-4}\begin{bmatrix} 8 + \sin(\pi t/125) + 2\sin(\pi t/200) \\ 5 - \sin(\pi t/125) - 3\cos(\pi t/200) \\ 6 + \sin(\pi t/125) + 5\cos(\pi t/200) \end{bmatrix} N$. The initial relative position and the desired target position vectors are set as $\boldsymbol{X}_{r0} = [14\ \ 25\ \ -5]^{\mathrm{T}}$ m and $\boldsymbol{X}_{rd} = [6\ \ -16.5\ \ 1]^{\mathrm{T}}$ m.

Case2: The radius of the sphere in collision avoidance potential and the external disturbances are set as $R = 15$ m and $\boldsymbol{d} = 10^{-3}\begin{bmatrix} 8 + \sin(\pi t/125) + 2\sin(\pi t/200) \\ 5 - \sin(\pi t/125) - 3\cos(\pi t/200) \\ 6 + \sin(\pi t/125) + 5\cos(\pi t/200) \end{bmatrix} N$. The initial relative position and the desired target position vectors are set as $\boldsymbol{X}_{r0} = [14\ \ 30\ \ -5]^{\mathrm{T}}$ m and $\boldsymbol{X}_{rd} = [13\ \ -19\ \ 0]^{\mathrm{T}}$ m.

4.1. **Simulation analysis of the anti-saturation controller.** For the situation of known upper bound of external disturbances, the parameters of the designed anti-saturation controller Equation (27) are selected as: $k_1 = 0.021$, $k_2 = 12$, $\tau_1 = 0.08$, $k_h = 40$, $k_{h1} = 0.8$, $k_\eta = 1.02$, $d_m = 0.05$. Simulation results of Case1 and Case2 using anti-saturation controller Equation (27) are shown in Figures 2-4.

The tracking error curves of $\boldsymbol{z}_1$ and $\boldsymbol{z}_2$ are given in Figures 2(a) and 2(b) respectively. The curves of all cases indicate that the position and velocity of chaser can converge in short time though there are external disturbances and input saturation, which satisfies the requirement of control accuracy. The control force curves of the system are provided in

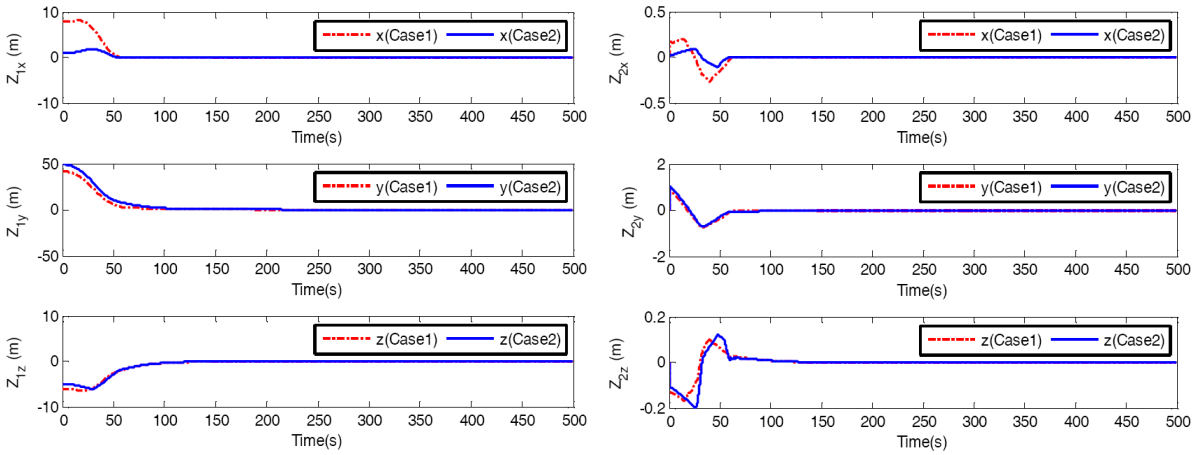

(a) The curves of tracking error $\boldsymbol{z}_1$ (b) The curves of tracking error $\boldsymbol{z}_2$

FIGURE 2. The curves of tracking error under the controller Equation (27)

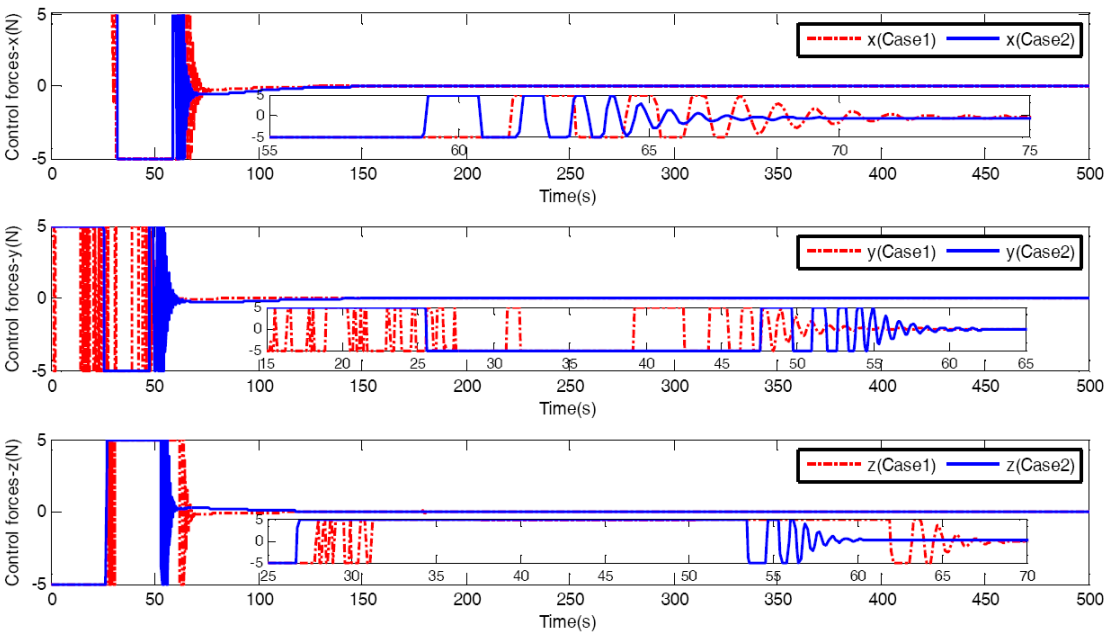

FIGURE 3. The control force curves of the system under the controller Equation (27)

Figure 3, from which it can be seen that the control forces are bounded in the whole control process without obvious chattering. Figure 4 shows the curve of potential function and the motion trajectory of chaser in the target orbit coordinate frame which describes the process of terminal approach more intuitively. Based on the results shown in Figures 4(a)-4(d), it can be known that there is no collision happening when the chaser approaches the target. Comparing the results of Case1 and the results of Case2 shows that the controller Equation (27) can realize the terminal safe approach with bigger difference of the external disturbances and taboo areas, which indicate the effectiveness and robustness of the controller Equation (27).

To verify the effectiveness of collision avoidance of the controller Equation (27) ($R = 15$ m), let $k_h = 0$, that is, the collision avoidance is not considered. The corresponding simulation results are shown in Figure 5. Based on the results, it can be seen that the

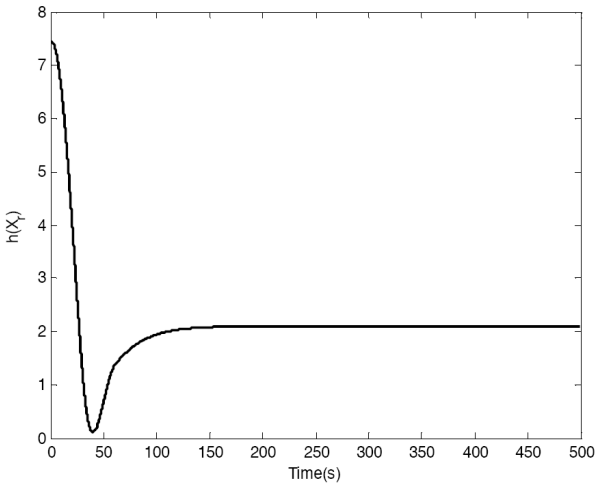

(a) The curve of potential function for Case1

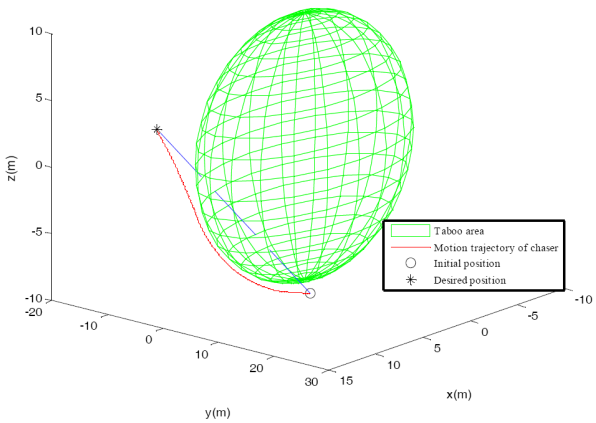

(b) The motion trajectory for Case1

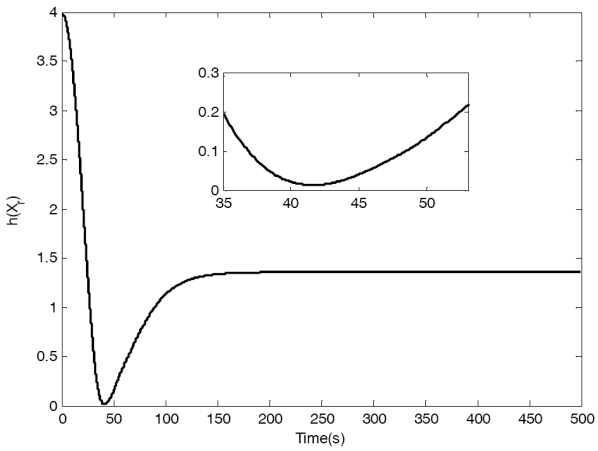

(c) The curve of potential function for Case2

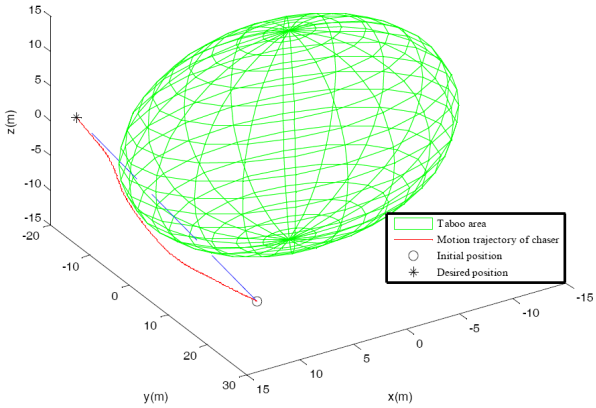

(d) The motion trajectory for Case2

FIGURE 4. The curves of potential function and motion trajectory of chaser under the controller Equation (27)

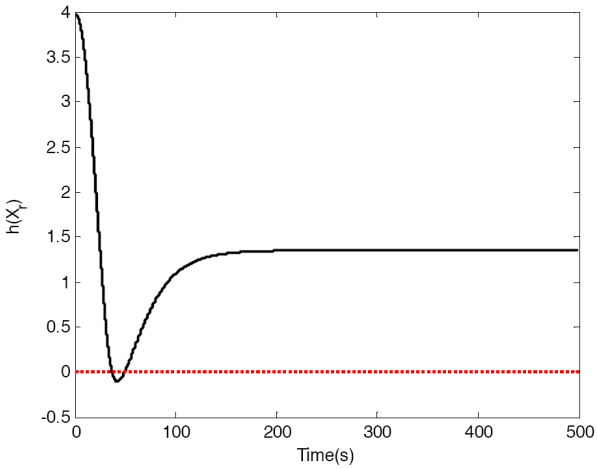

(a) The curve of potential function

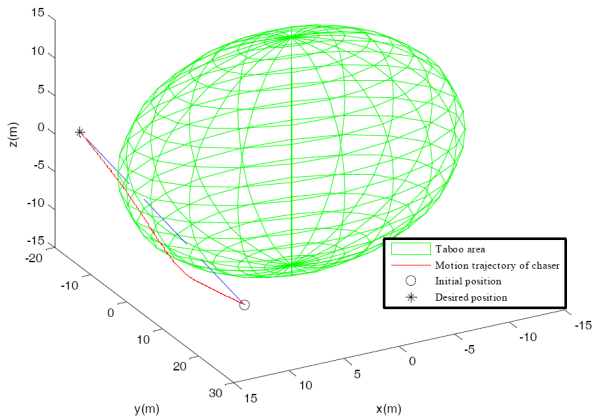

(b) The motion trajectory of chaser

FIGURE 5. Simulation results using the controller Equation (27) with $k_h = 0$

chaser collides with the target in the process of terminal approach if the collision avoidance is not considered in controller design. Compared with Case2, it further indicates that the controller Equation (27) is useful for collision avoidance.

According to the above analysis, for the situation that the upper bound of the external disturbances is known, the results presented in Figures 2-5 indicate that the anti-saturation controller Equation (27) is effective for the chaser to realize the terminal approach without collision.

4.2. **Simulation analysis of the adaptive anti-saturation controller.** For the situation of unknown upper bound of external disturbances, the parameters of the designed adaptive anti-saturation controller Equation (34) are selected as: $k_1 = 0.033$, $k_2 = 18$, $k_3 = 0.0004$, $\tau_1 = 0.05$, $k_h = 40$, $k_\eta = 1.8$, $\gamma_d = 0.4$. Simulation results of Case1 and Case2 using adaptive controller Equation (34) are shown in Figures 6-9.

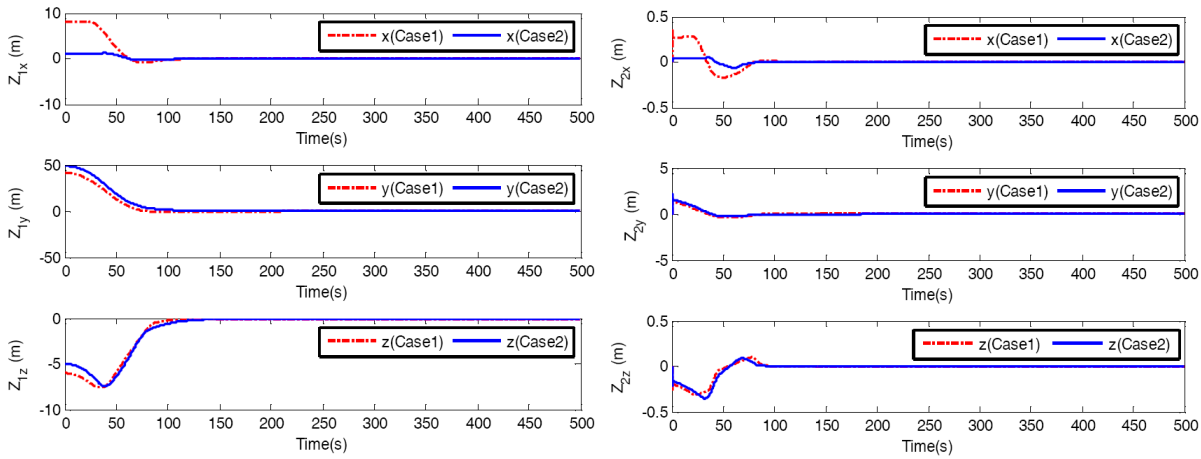

(a) The curves of tracking error $\boldsymbol{z}_1$ (b) The curves of tracking error $\boldsymbol{z}_2$

FIGURE 6. The curves of tracking error under the controller Equation (34)

In Figure 6(a) and Figure 6(b), the tracking error curves of $\boldsymbol{z}_1$ and $\boldsymbol{z}_2$ are given respectively for two cases. From the simulation curves, it can be seen that the position and the velocity of chaser can converge in short time satisfying the requirement of control accuracy regardless of external disturbance, parameter uncertainty and input saturation of the system. The control force curves of the system presented in Figure 7 show that the control forces are bounded in the whole control process without chattering which satisfy the requirement of input constraint, and the control forces are better than the control forces in Figure 3. The curves of adaptive parameters shown in Figure 8 manifest that the estimated values $\hat{d}_m$ approach a steady value after a period of time, which indicates that the adaptive schemes are effective to estimate the value of the upper bound of unknown external disturbances d_m. Figure 9 gives the curve of potential function and the motion trajectory of chaser in the target orbit coordinate frame, which shows that the value of the potential function is positive and the chaser can accomplish terminal approach being away from the taboo area for two cases. Analyzing the results above, it can be seen that the controller Equation (34) can realize the terminal safe approach for the two cases with difference of the external disturbances and taboo areas, which indicate the effectiveness and robustness of the controller Equation (34).

To verify the effectiveness of collision avoidance of the adaptive controller Equation (34) ($R = 15$ m), let $k_h = 0$, the corresponding simulation results are shown in Figure 10. From the results, it can be seen that the chaser collides with the target during terminal

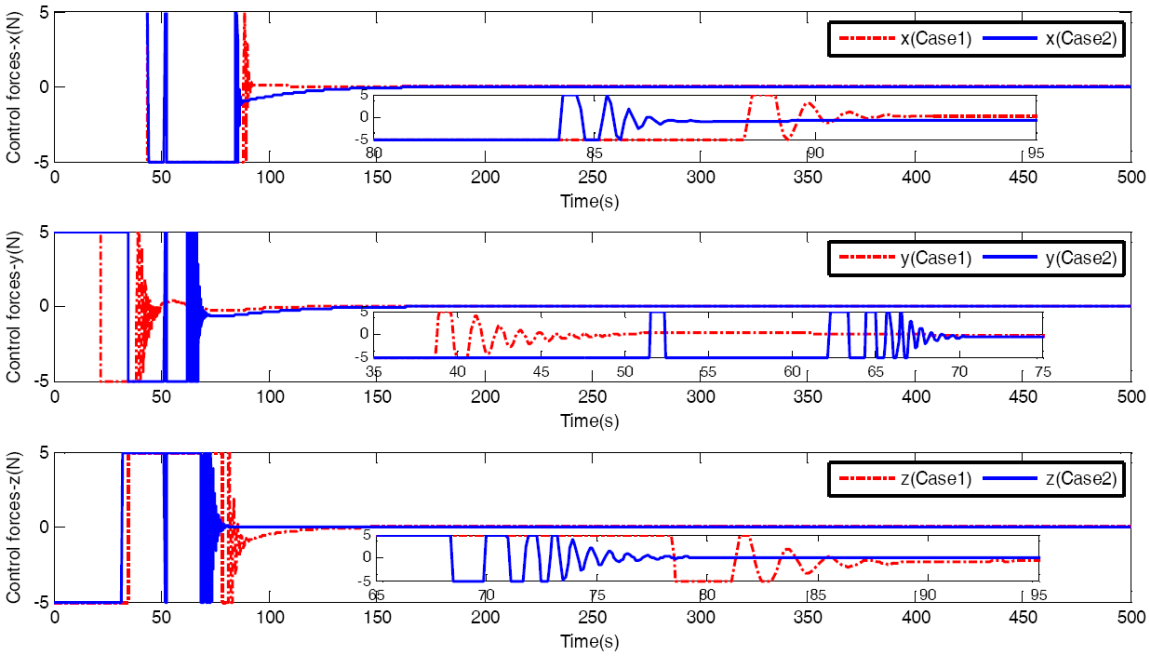

FIGURE 7. The control force curves of the system under the controller Equation (34)

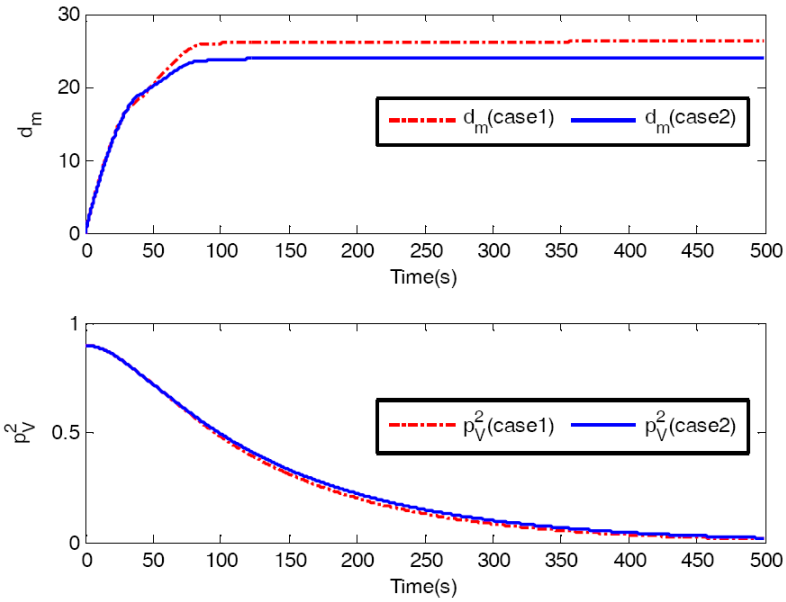

FIGURE 8. The curves of adaptive parameters under the controller Equation (34)

approach if the collision avoidance is not taken into account, which further indicate that the controller Equation (34) is effective to avoid collision in terminal approach.

All in all, for the situation that upper bound of the external disturbances is unknown, the results presented in Figures 6-10 indicate that the adaptive anti-saturation controller Equation (34) is effective for the chaser to realize the terminal safe approach.

5. **Conclusions.** The anti-saturation control strategies for spacecraft terminal safe approach are researched in this paper based on DSC, auxiliary system and spherical collision

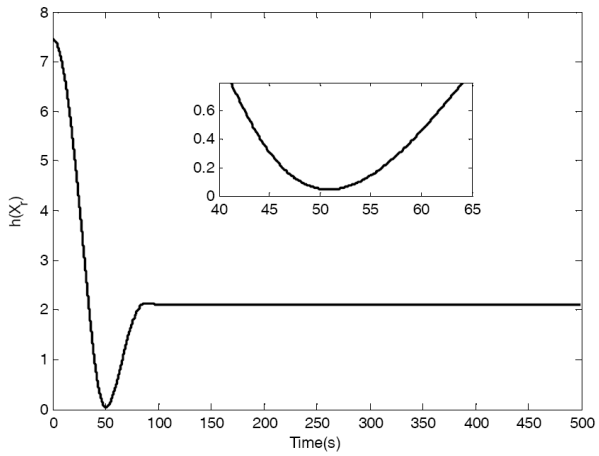

(a) The curve of potential function for Case1

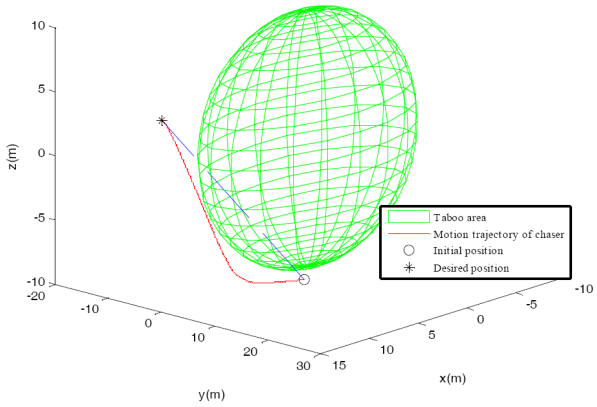

(b) The motion trajectory for Case1

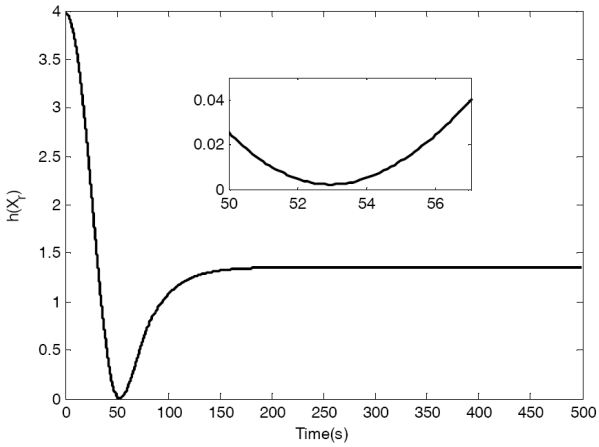

(c) The curve of potential function for Case2

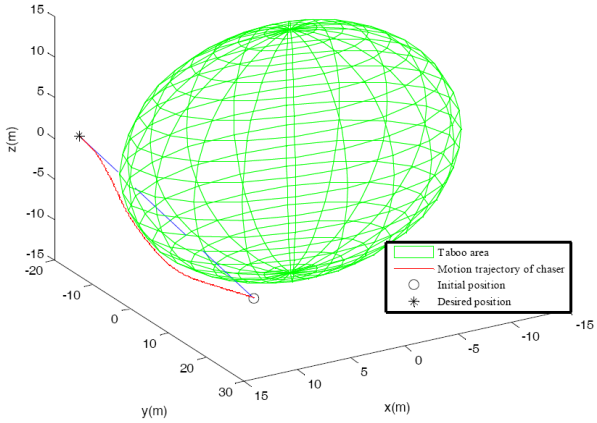

(d) The motion trajectory Case2

FIGURE 9. The curves of potential function and motion trajectory of chaser under the controller Equation (34)

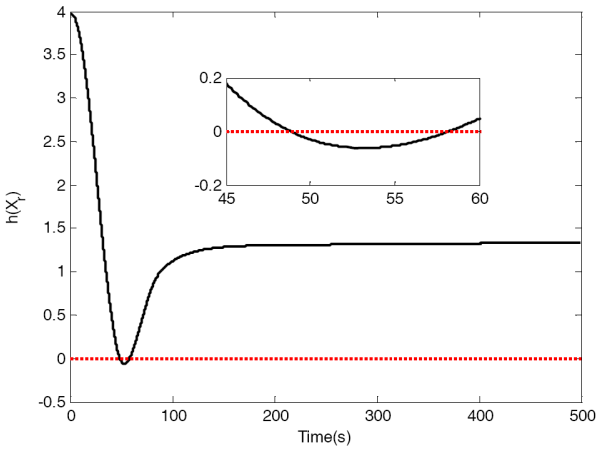

(a) The curve of potential function

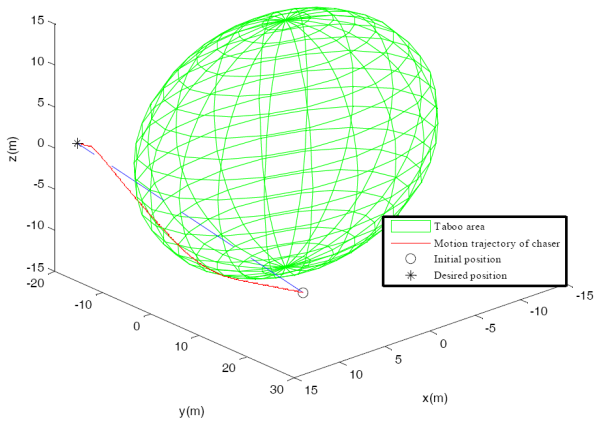

(b) The motion trajectory of chaser

FIGURE 10. Simulation results using the controller Equation (34) with $k_h = 0$

avoidance potential function. According to the theoretical proofs and numerical simulations, conclusions are drawn as follows.

(1) The safety problem of terminal approach control is simplified into boundedness problem of the reciprocal of the potential function by introducing the spherical collision avoidance potential function.

(2) For the situations of known and unknown upper bound of external disturbances, two novel anti-saturation control schemes for spacecraft terminal safe approach are put forward. The first-order command filter is used to avoid the differential of the virtual control signals, and the effect of the error caused by the command filter can be removed by introducing the compensating signals.

(3) Under the designed controllers, the states of system are bounded and uniformly ultimately bounded respectively, and the tracking errors can converge to any small neighborhood. Also the chaser spacecraft can approach the expected position safely. The numerical simulation results further indicate the effectiveness of the designed controllers.

Acknowledgment. The authors would like to acknowledge the support provided by the China Aerospace Science and Technology Innovation Foundation (CAST. No. JZ201600 08), the State Key Program of National Natural Science Foundation of China (61333003) and the Major Program of Natural Science Foundation of China (61690210).

REFERENCES

[1] C. Guariniello and D. A. DeLaurentis, Maintenance and recycling in space: Functional dependency analysis of on-orbit servicing satellites team for modular spacecraft, *AIAA SPACE 2013 Conference and Exposition*, pp.1-16, 2013.

[2] E. Capello, E. Punta, F. Dabbene et al., Sliding-mode control strategies for rendezvous and docking maneuvers, *Journal of Guidance, Control, and Dynamics*, vol.40, no.6, pp.1481-1488, 2017.

[3] S. Di Cairano, H. Park and I. Kolmanovsky, Model predictive control approach for guidance of spacecraft rendezvous and proximity maneuvering, *International Journal of Robust and Nonlinear Control*, vol.22, no.12, pp.1398-1427, 2012.

[4] B. Zhou, Z. L. Lin and G. R. Duan, Lyapunov differential equation approach to elliptical orbital rendezvous with constrained controls, *Journal of Guidance, Control, and Dynamics*, vol.34, no.2, pp.345-358, 2011.

[5] S. N. Wu, Z. G. Wu, G. Radice et al., Adaptive control for spacecraft relative translation with parametric uncertainty, *Aerospace Science and Technology*, vol.31, no.1, pp.53-58, 2013.

[6] X. Huang, Y. Yan, Y. Zhou et al., Sliding mode control for Lorentz-augmented spacecraft hovering around elliptic orbits, *Acta Astronautica*, vol.103, pp.257-268, 2014.

[7] L. Cao and X. Q. Chen, Input-output linearization minimum sliding-mode error feedback control for spacecraft formation with large perturbations, *Proc. of the Institution of Mechanical Engineers, Part G: Journal of Aerospace Engineering*, vol.229, no.2, pp.352-368, 2015.

[8] K. W. Xia and W. Huo, Robust adaptive back-stepping neural networks control for spacecraft rendezvous and docking with uncertainties, *Nonlinear Dynamics*, vol.84, no.3, pp.1683-1695, 2016.

[9] D. W. Zhang, S. M. Song and R. Pei, Safe guidance for autonomous rendezvous and docking with a non-cooperative target, *AIAA Guidance, Navigation, and Control Conference*, pp.1-19, 2010.

[10] Q. L. Hu, H. Y. Dong, Y. M. Zhang et al., Tracking control of spacecraft formation flying with collision avoidance, *Aerospace Science and Technology*, vol.42, pp.353-364, 2015.

[11] L. Palacios, M. Ceriotti and G. Radice, Close proximity formation flying via linear quadratic tracking controller and artificial potential function, *Advances in Space Research*, vol.56, no.10, pp.2167-2176, 2015.

[12] L. C. Feng, Q. Ni, Y. Z. Bai et al., Optimal sliding mode control for spacecraft rendezvous with collision avoidance, *IEEE Congress on Evolutionary Computation (CEC)*, pp.2661-2668, 2016.

[13] J. Chen, M. G. Gan, J. Huang et al., Formation control of multiple Euler-Lagrange systems via null-space-based behavioral control, *Science China Information Sciences*, vol.59, no.1, pp.1-11, 2016.

[14] M. Leomanni, E. Rogers and S. B. Gabriel, Explicit model predictive control approach for low-thrust spacecraft proximity operations, *Journal of Guidance, Control, and Dynamics*, vol.37, no.6, pp.1780-1790, 2014.

[15] A. Weiss, M. Baldwin, R. S. Erwin et al., Model predictive control for spacecraft rendezvous and docking: Strategies for handling constraints and case studies, *IEEE Trans. Control Systems Technology*, vol.23, no.4, pp.1638-1647, 2015.

[16] H. Park, C. Zagaris, J. Virgili-Llop et al., Analysis and experimentation of model predictive control for spacecraft rendezvous and proximity operations with multiple obstacle avoidance, *AIAA/AAS Astrodynamics Specialist Conference*, pp.1-17, 2016.

[17] M. Chen, S. S. Ge and B. B. Ren, Adaptive tracking control of uncertain MIMO nonlinear systems with input constraints, *Automatica*, vol.47, no.3, pp.452-465, 2011.

[18] H. Q. Wang, B. Chen, X. P. Liu et al., Robust adaptive fuzzy tracking control for pure-feedback stochastic nonlinear systems with input constraints, *IEEE Trans. Cybernetics*, vol.43, no.6, pp.2093-2104, 2013.

[19] Q. Zhou, L. J. Wang, C. W. Wu et al., Adaptive fuzzy control for nonstrict-feedback systems with input saturation and output constraint, *IEEE Trans. Systems, Man, and Cybernetics: Systems*, vol.47, no.1, pp.1-12, 2017.

[20] F. Wang, Q. Zou and Q. Zong, Robust adaptive back-stepping control for an uncertain nonlinear system with input constraint based on Lyapunov redesign, *International Journal of Control, Automation and Systems*, vol.15, no.1, pp.1-14, 2017.

[21] Q. Wang, B. Zhou and G. R. Duan, Robust gain scheduled control of spacecraft rendezvous system subject to input saturation, *Aerospace Science and Technology*, vol.42, pp.442-450, 2015.

[22] L. Sun, W. Huo and Z. X. Jiao, Adaptive backstepping control of spacecraft rendezvous and proximity operations with input saturation and full-state constraint, *IEEE Trans. Industrial Electronics*, vol.64, no.1, pp.480-492, 2017.

[23] J. P. Yu, P. Shi, W. J. Dong et al., Observer and command-filter-based adaptive fuzzy output feedback control of uncertain nonlinear systems, *IEEE Trans. Industrial Electronics*, vol.62, no.9, pp.5962-5970, 2015.